IEEE Open Journal of
Intelligent Transportation
Systems

Received 3 April 2020; revised 9 July 2020 and 21 August 2020; accepted 24 August 2020. Date of publication 26 August 2020; date of current version 23 September 2020.

Digital Object Identifier 10.1109/OJITS.2020.3019599

An All-Electric Alpine Crossing: Time-Optimal Strategy Calculation via Fleet-Based Vehicle Data

MAXIMILIAN CUSSIGH [1], TOBIAS STRAUB [2], MICHAEL FREY [2], THOMAS HAMACHER [1], AND FRANK GAUTERIN [2]

[1]Chair of Renewable and Sustainable Energy Systems, Technical University of Munich, 85748 Garching, Germany

[2]Institute of Vehicle System Technology, Karlsruhe Institute of Technology, 76131 Karlsruhe, Germany

CORRESPONDING AUTHOR: T. STRAUB (e-mail: tobias.straub@partner.kit.edu)

This work was supported by the KIT-Publication Fund of the Karlsruhe Institute of Technology. *(Maximilian Cussigh and Tobias Straub are co-first authors.)*

ABSTRACT Recently, individual electric mobility gains significance due to legislation and social discussion. Customers demand longer battery ranges. Advanced planning is a different and more sustainable approach. Potentially, they assist drivers in exploiting the installed range on long journeys. Earlier research of the authors showed that an optimal combination of speed, charging choice and amount potentially reduces overall traveling time on long trips. In this work, a dynamic programming algorithm controls this strategy set time-optimally on an all-electric route from Munich to Verona. For this, location-specific fleet-based data of over 600 000 km are used to improve the reliability of the strategy set in two ways. Firstly, the data provide more realistic location- and time-specific velocity bounds for speed control. Secondly, they provide fleet-sourced dynamics to a traceable analytical consumption model. These additional dynamics lead to 1.8 - 2.3 % more energy demand in the strategy planning compared to a less accurate consumption map-based approach. Here, the incorporation of dynamics increases the optimizations' reliability. Also, the time-dependent fleet-data allows finding an optimal departure time for the given route. In total, the incorporation of fleet information enhances the robustness of the optimization. This enables a more seamless experience of electric mobility on long trips.

INDEX TERMS Electric vehicles, smart mobility, dynamic programming, fleet data, consumption modeling.

NOMENCLATURE

LATIN SYMBOLS

A	Frontal area
a	Acceleration
c_x	Drag coefficient
E	Energy
e	Specific consumption
e_{rot}	Rotational mass factor
F	Force
f_{rel}	Relative frequency
f_{t}	Rolling resistance
g	Gravitational acceleration
H	Upper velocity bound
L	Lower velocity bound
m	Number of segments
m_{veh}	Vehicle mass
n	Number of charging events
P	Power
p_{vec}	Parameter vector
r	Charging load
r_{vec}	Route vector
s	Distance
t	Time
v	Vehicle speed

GREEK SYMBOLS

α	Slope
γ	Charge gradient
η_{DT}	Drive train efficiency
τ	Travel time
ρ	Air density

The review of this article was arranged by Associate Editor Bilge Atasoy.

SUBSCRIPTS

DT	Drivetrain
End	End
HVB	High voltage battery
i	Index i
M	Modified fleet-distribution for given velocity
max	Maximum
min	Minimum
nom	Nominal
O	Original fleet-distribution for median velocity

SUPERSCRIPTS

k	Grid index state variable energy
l	Grid index control variable charging load
w	Grid index control variable velocity

ACRONYMS

BEV	Battery electric vehicle
CM	Charging model
DI	Dynamic interval of percentiles to derive velocity windows from fleet
DP	Dynamic program
DPMA	Driving profile map attribute
DPMAD	Driving profile map attribute distribution
EC	Energy consumption
ECM	Energy consumption map
EPF	Fleet data-based EC prediction framework
HVB	High voltage battery
IA	Integral acceleration
ID	Identification number of map link
IAP	IA while propulsion, one DPMA
IAR	IA while recuperation, one DPMA
ISV	Integral squared velocity
ISVP	ISV while propulsion, one DPMA
ISVR	ISV while recuperation, one DPMA
MINLP	Mixed-integer non-linear program
P	Propulsion
R	Recuperation
RSME	Root mean square error
SOC	State of charge
VW	Velocity window.

I. INTRODUCTION

PERSONAL vehicle-based mobility is subject to a paradigm shift. Among other aspects, the aim of reducing carbon dioxide and rising regulations for fossil fuel-based vehicles push the share of (fully) electric transport. For personal transportation, battery electric vehicles (BEVs) mostly come along with limited driving ranges in comparison to conventional vehicles. Although, the mean daily mileage of a vehicle in Germany is 37 km [1], there is a customer's demand for higher ranges. This desire is mainly addressed by enlarging the batteries' capacity. However, their production is neither economically nor ecologically sustainable, e.g., due to battery cost of at least 100 USD per kW h [2] and to use of scarce resources. In turn, when keeping battery sizes small, especially long trips become time consuming due to more frequent charging events. The minimization of total travel time thus becomes more complex. For this, an optimal strategy planning algorithm can be applied for a given long-distance driving task. In this article, long-distance driving are defined by at least one recharging event along the route.

For providing a time-optimal journey to the driver of a BEV, planning must incorporate vehicle-specific sensitivities adequately. Apart from the charger selection along a given route, an appropriate choice of the vehicle speed enables the additional potential to minimize total traveling time. For instance, it is then possible to minimize or optimize necessary charging stops by adapting speed. To the current knowledge, conventional routing algorithms do not include these levers. Also, for the application of optimal strategies to real driving use cases, prediction models for energy consumption (EC) and charging time have to be sufficiently exact and reliable.

The optimal planning of a charging strategy is extensively examined in the literature. However, conventional routing problems need adaptions for a BEV implementation. Artmeier *et al.* were the first formulating appropriate changes by using an energy graph network [3]. Based on that, preprocessing reduces query times significantly in [4]. Mainly, the optimal choice of charging stations is modeled as a shortest path problem (SPP) in [5]–[8]. Except [7] using a more elaborated model including recurring accelerations, all these shortest path problem approaches are based on a physical model or a consumption map. Another approach uses a mixed-integer non-linear program (MINLP) formulation, that [9] and [10] use to optimize driving tasks in a heterogenous charger network. There, vehicle consumption relies on a single constant, only dependent on the segment length, independent from speed and elevation.

All these optimization algorithms lack the vehicle speed as a further control lever. A trade-off between energy consumption and speed is firstly presented in [11] by using pareto-optimal routes with homogeneous recharging nodes without the optimization of charging energies. Additionally, [12] adds charging energy planning to the charger and velocity selection using dynamic programming. The basis for [11] is a physical vehicle consumption model and for [12] a consumption map model.

For the input of consumption prediction, there are various types of approaches. So-called direct methods use recorded ECs for prediction either road-segment specific [13] or clustered by road class [14]. Still, EC is not only location-specific. For the incorporation of varying influences like velocity, [12] use a consumption map and [15]–[17] use machine learning. However, all of them lack physical traceability and need to be trained for each vehicle separately. In turn, analytical EC models can provide both based on the driving resistance equation [18]–[20]. Thus, most beneficial is an analytical approach. It is physically traceable and adaptable, and can correctly incorporate varying influences.

Apart from their type, the models above differ in their input origin. Two input classes exist. Firstly, map-based models use segment-specific information like speed limits and road type [17], [19], [21]. Secondly, there are spatially limited models only using ego-vehicle data [16] and other approaches consider fleets [15]. The latter enlarge the prediction area spatially. The broader the vehicle-based data, the better these models can consider location-specific influences on EC. Accordingly, there is no need to reconstruct vehicle behavior from map information. Thus, additional uncertainties are avoided. Consequently, an analytical EC prediction model by [20] using fleet data is the most favorable.

The present paper firstly combines a driving and charging strategy optimization algorithm first published in [12] with a fleet-based analytical EC model firstly presented in [20], called energy prediction framework (EPF). The optimization combines the selection of charging stations and energies with a dynamic speed adaption along a given route in a heterogenous charger network [12]. The DP-based algorithm is extended and further assessed. This includes four novelties. Firstly, a sensitivity analysis in terms of spatial discretization and its effects on performance and solution quality is investigated. Secondly, static velocity bounds for route segments are replaced with dynamic, time- and location-specific velocity constraints based on fleet-data. This also includes a variation in the width of the resulting velocity window per route segment. Fleet-based velocity bounds guarantee a more realistic and applicable strategy planning. Thirdly, the impact of time dependency in the velocity bounds is investigated by varying the time of departure for one representative day. This is possible because fleet information reflects daytime dependent changes in traffic. Fourthly, in addition to a previously examined energy consumption map (ECM) model in [12], the energy consumption is analytically modeled using a fleet-sourced data basis [20] and thus including dynamics. Moreover, this work presents a novel method to adapt the fleet-based energetic information for a velocity selected by the optimizer. To the authors' knowledge, this is the first time in literature, that a fleet-based EPF provides realistic velocity bounds to the optimization algorithm and energy consumption information, which includes location-specific dynamics for a given long-distance journey scenario.

II. METHODS & MATERIALS

The optimization of charger choice, charged energy and vehicle speed adaption for a given route is fed with charging time by a charging model and consumption information by two different EC models. In the present chapter, the overall method approach including the optimization algorithm, the two EC models and a charging model, are presented. Both the optimization and consumption models are then illustrated in detail. Finally, an exemplary route scenario is presented.

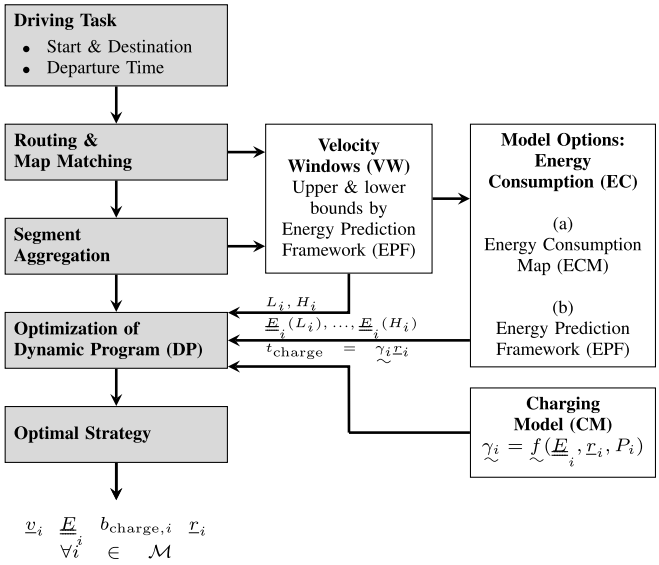

FIGURE 1. Method approach in driving strategy optimization via DP with two input models (white): energy prediction and charging time.

A. METHOD OVERVIEW

The calculation of an optimal strategy set for a given driving task bases on fleet-sourced input models. Fig. 1 illustrates this process.

After the driving task is set, the route's course is calculated with the help of a programming interface of a routing service provider. For further information, see [22]. This route is then matched to a more detailed map. This is owned by the research partner BMW Group and its suppliers. Therefore it is assumed as a validated and given input. The fleet-based energy prediction approach rests on this detailed data. The matching on this map is built on a Hidden Markov model, as outlined by [23]. This map can describe the route by the sum of its smallest bits, the links. Each link has a specific identification number (ID). Based on this ID, the presented approach uses each link's length, speed limit and a mean slope. For each link's specific energy prediction, the link IDs and their properties are firstly processed in order to determine fleet-based velocity windows (VWs). Here, a fleet-based energy prediction framework (EPF) identifies a lower and upper-velocity border for every link. Then, the link IDs and VWs are transferred to an energy consumption (EC) model. Two different models are then implemented and compared. These are an energetic consumption map (ECM) and the fleet-based EPF. This comparison examines differences in the models' impact on the optimal strategy calculation. Before the information on vehicle speed and energy consumption is fed into the optimizer, the individual links and their information are aggregated to larger segments with a nominal maximal length Δs_{nom} (see Section II-E). These segments can consist of multiple links. The EC's output are segment-individual VWs with segment-specific minimal (L_i) and a maximum (H_i) thresholds. Based on these velocity thresholds, corresponding energy consumption

values $\underline{\underline{E}}_i$ per aggregated segment i are given to the optimizer. Double underline indicates the state variable of the following optimization problem in Section II-B. For charging events within the optimization, the given charging model (CM) calculates the necessary charging time t_{charge} for the energy amount that is demanded by the optimizer. The optimization takes this EC and CM information for each segment to calculate a set of time-optimal speeds $\underline{v}_i$, energy consumption $\underline{\underline{E}}_i$, charging decisions $b_{\text{charge},i}$ and charging energies $\underline{r}_i$. This is done for all segments $i \in \mathcal{M}$. A single underline marks the two control variables of the following optimization problem.

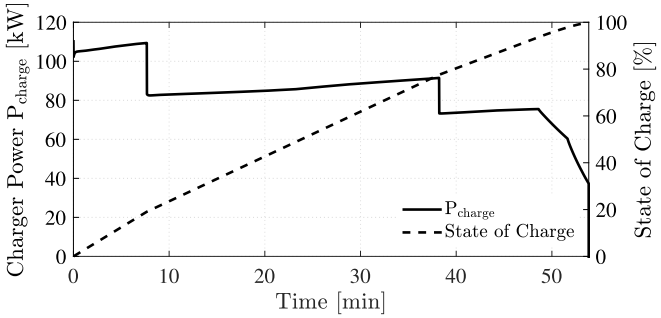

FIGURE 2. Course of vehicle charger power with an infrastructural nominal peak of 120 kW (solid) and the course of the state of charge (dashed).

B. TIME-OPTIMAL STRATEGY CALCULATION

The optimization of the driving task is based on a dynamic programming algorithm. This originates from work of [24]. For more in-depth information on the topic see [25]. The present considerations for optimization of driving and charging strategies mainly base on [12]. There and also in the present paper, a way based optimization via dynamic programming using [26] is executed to guarantee a minimal total travel time. The underlying problem is modeled with a singular state variable, two control variables and a fixed final state. Double underline marks the state variable, single underline the control variables and the wave the non-linear input models. The optimization problem can thus be formulated as

$$\min_{\underline{v}_{i,i+1},\underline{r}_i,\ i\in\mathcal{M}} \quad \sum_{i=1}^{m} \tau_{i,i+1}(\underline{v}_{i,i+1}) + \underline{r}_i\underset{\sim}{\gamma}_i \tag{1}$$

subject to

$$\underline{\underline{E}}_{i+1} = f(\underline{\underline{E}}_i, \underline{r}_i, \underline{v}_{i,i+1}) \tag{2}$$

$$\underset{\sim}{\gamma}_i = f(\underline{\underline{E}}_i, \underline{r}_i, P_i) \tag{3}$$

$$\Delta\underline{\underline{E}}_i = \underline{\underline{E}}_i^{k} - \underline{\underline{E}}_i^{k-1} \tag{4}$$

$$\Delta\underline{r}_i = \underline{r}_i^{l} - \underline{r}_i^{l-1} \tag{5}$$

$$\Delta\underline{v}_i = \underline{v}_i^{w} - \underline{v}_i^{w-1} \tag{6}$$

$$\underline{\underline{E}}_i \in [E_{\min}, E_{\min} + \Delta\underline{\underline{E}}_i, \ldots, E_{\max}] \tag{7}$$

$$E_m \in [E_{\text{End}}, E_{\text{End}} + \Delta\underline{\underline{E}}_i] \tag{8}$$

$$\underline{r}_i \in [0, 0 + \Delta\underline{r}_i, \ldots, E_{\max} - E_{\min}] \tag{9}$$

$$\underline{v}_i \in [L_{i,i+1}, L_{i,i+1} + \Delta\underline{v}_i, \ldots, H_{i,i+1} - \Delta\underline{v}_i, H_{i,i+1}] \tag{10}$$

$$E_1 \text{ given}, \quad r_1 = r_m = 0 \tag{11}$$

The system's behavior in the underlying problem of optimizing a given driving task is described through the state variable $\underline{\underline{E}}_i$ in (2). It describes the high voltage battery's (HVB's) energy. For the driving task, the battery's energy at the beginning and the end of the task is set in (8) and (11). By that, running out of energy is prevented through a threshold. In the present case, these thresholds are 100 % SOC for E_1 in (11) and 20 % for E_{end} in (8). Both control variables $\underline{r}_i$ and $\underline{v}_{i,i+1}$ determine the desired minimization of the overall driving time in (1) per step i. The controls represent the amount of energy $\underline{r}_i$ being charged at a charging station and the driving velocity $\underline{v}_{i,i+1}$ from vertex i to $i+1$. Both are limited through further constraints in (9) and (10) respectively. The charging energy $\underline{r}_i$ can range from zero (no charging) to full charge. The latter is the difference of the battery's total energy $E_{\max}$ and a minimal amount of energy $E_{\min}$ that is never to be undercut in (7). The constraints for the realized speeds in (10) are determined through energetic fleet data. The charger specific power characteristic is modeled through $\underset{\sim}{\gamma}_i$ and is a non-linear function (3) of $\underline{r}_i$ and $\underline{\underline{E}}_i$ (see Fig. 2). The wave indicates this non-linearity, same with the system's model equation (2). Due to the discrete character of dynamic programming, the state variable as well as both controls are evaluated on an individually scaled discrete grid. The grids' sizes for the state of charge (SOC), the charged SOC and the vehicle speed are $\Delta\underline{\underline{E}}_i = 0.5\,\%$ SOC, $\Delta\underline{r}_i = 0.5\,\%$ SOC and $\Delta\underline{v}_i = 1\,\text{km/h}$, respectively. The position of a value at index i within these multidimensional and discrete grids is described by indices k, l and w. They are defined in (4), (5) and (6). Overall, the cost function (1) minimizes the overall traveling time within the given boundaries according to this works objective. Further optimization objectives such as battery aging, e.g., battery currents, could be included in the cost function (1) in future work.

C. CHARGING MODEL

Charging a vehicle at high powers with direct current results in a non-linear function $t_{\text{charge}} = \underline{r}_i\underset{\sim}{\gamma}_i$ due to thermal limitations and physical behavior of the high voltage battery system [27]. For the calculation of the charging time in (1), the non-linear charging functions $\underset{\sim}{\gamma}_i$ in (3) for different power levels are defined. For a charging process of 120 kW, Fig. 2 shows the course of the charging power and the battery's SOC. The degressive behavior of the SOC for higher values is visible. Also, the time versus SOC curve is, especially for higher charging powers, non-linear. The relevant chargers in Section II-G have nominal power levels from 50 to 120 kW. The corresponding charging curves come from a

given total vehicle simulation environment, implemented in Modelica. They are approximated by a polynomial of fourth order for (1) whose accuracy is expressed by an RMSEs (Root Mean Square Error) of 0.47 % SOC.

D. ENERGY CONSUMPTION PREDICTION MODELS

In the present paper, two EC models are used as input for optimization. Fig. 1 depicts these. The fleet-sourced EPF always provides the link-specific realized VWs, whereas two different approaches model the EC input for the optimizer. Firstly, the speed-dependent ECM uses the velocity data from the EPF to calculate ECs. In the second approach, to compare the impact of energetic fleet information, the EPF predicts the ECs within the set VWs.

The ECM models the consumption as a function of speed and slope, i.e., $e_i(\underline{v}_i, \alpha_i)$. It is based on the simulated consumption output of the same Modelica-based total vehicle simulation that is used for the charging model. A polynomial of sixth-degree approximates the simulated consumed energy as a function of vehicle speed. This results in an accuracy of an RMSE of 0.7 $\frac{\%\ \text{SOC}}{100\text{km}}$. The resulting ECM is dependent on a constant vehicle speed $\underline{v}_{ij}$ and the slope α_{ij} of a road segment. Here, no dynamics due to acceleration effects are considered.

In turn, the EPF bases on [20] with adaptions due to optimizer requirements which the following and Section II-F describe.

Equation (12) describes a route's EC $E_{\text{HVB,m}}$ at the connector of the HVB. $E_{\text{HVB,m}}$ is the sum of the EC of the drive train and auxiliary consumers for the entire route. For the drive train's EC, the wheel force F_W is integrated over distance s, whereby the operating point dependent drivetrain efficiency η_{DT} needs to be set according to the energy's flow. Here, the flow determines the sign of F_W. It is either positive for an energy demand by the drive train, i.e., propulsion (P), or negative in case of recuperation (R). The calculation of F_W is described in (13). It represents the sum of the vehicle's driving resistance forces. Under the assumption of quasi-static states within each segment, (13) separately depicts the mainly vehicle-related parameters in the parameter vector $\vec{p}$. These are aerodynamic drag coefficient c_x, air density ρ, frontal area A, gravity's acceleration g, rotational mass factor e_{rot}, tire rolling resistance coefficient f_t and vehicle mass m : veh. Additionally the route vector $\vec{r}$ contains the inclination α and the driving profile represented by velocity v and acceleration a.

Similar to the drive train's EC, the auxiliary consumers are also assumed quasi-statically. This means that their power demand $P_{\text{Aux},i}$ in (12) is constant along a segment. This power demand is also influenced by the surrounding temperature. In this work it is set constant. Prospectively, a weather forecast based model can predict this demand more detailed. The length of segment Δs_i is part of the map information, and the average speed $\bar{v}_i$ (AV) is also known

TABLE 1. Energetic driving profile map attributes (DPMAs) from [20].

	Propulsion	Recuperation
Integral **A**cceleration	**IAP**: $\int [a(s)]_{\text{P}} ds$	**IAR**: $\int [a(s)]_{\text{R}} ds$
Integral **S**quared **V**elocity	**ISVP**: $\int [v^2(s)]_{\text{P}} ds$	**ISVR**: $\int [v^2(s)]_{\text{R}} ds$
Average **V**elocity	**AV**: $\bar{v}$	

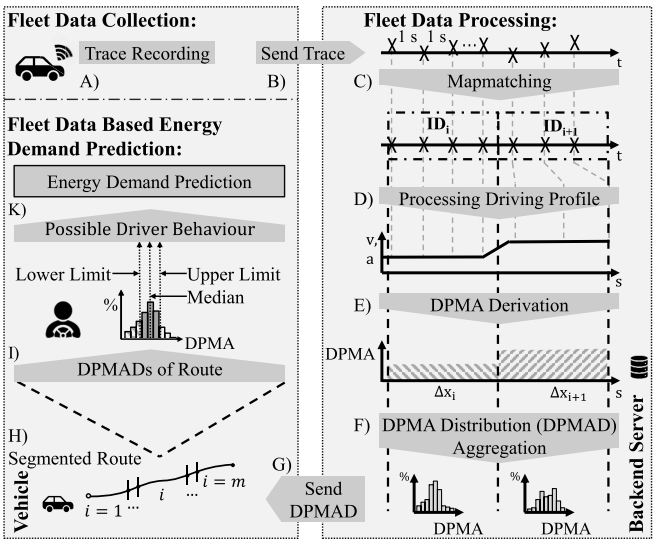

FIGURE 3. Fleet data-based energy consumption prediction framework (EPF) adapted from [20].

for the calculation of the expected duration on a segment.

$$E_{\text{HVB},m} = \sum_{i=1}^{m} \int_{i}^{i+1} \frac{F_{\text{W}}(s)}{\eta_{\text{DT}}^{sgn(F_{\text{W}}(s))}} ds + P_{\text{Aux},i} \cdot \frac{\Delta s_i}{\bar{v}_i} \quad (12)$$

$$F_{\text{W}}(s) = \vec{p}_{\text{vec}}^{\,T} \cdot \vec{r}_{\text{vec}} = \begin{pmatrix} m_{\text{veh}} \cdot e_{\text{rot}} \\ \frac{\rho}{2} \cdot c_{\text{x}} \cdot A \\ f_{\text{t}} \cdot m \cdot g \\ m \cdot g \end{pmatrix}^{T} \cdot \begin{pmatrix} a(s) \\ v^2(s) \\ \cos(\alpha) \\ sin(\alpha) \end{pmatrix} \quad (13)$$

When extracting only the driving profile's influence from (12) and (13), this results in the energetic driving profile map attributes (DPMAs) shown in Table 1. Note that the integral DPMAs have to be split corresponding to the direction of the energy's flow. This separation in propulsion and recuperation is necessary in order to consider η_{DT} correctly. Just the average velocity (AV), as the auxiliary EC is independent of η_{DT}.

Fig. 3 shows the procedure of the EPF to collect the inferred DPMA in steps A) until I), which differs in the last steps from the one presented in [20] according to the requirements of the optimizer. Two boxes propose different computation locations on a backend server and in the vehicle. The fleet vehicles record A) anonymized fragments of traces of geo-positions and timestamps. The fleet consists of heterogeneous vehicles as the resulting data-set provides more data on a given route. The vehicle sends B) them to a backend server. The server matches the traces of multiple vehicles to a map C) and reconstructs their driving profile D). From these driving profiles and for each traversed segment, the backend obtains the energetic DPMAs E). These segments are limited

to 50 m length. In F) the backend groups the DPMAs for each segment and similar recording daytime and weekdays to obtain driving profile map attribute distributions (DPMADs). The overall set of DPMADs constitutes an energetic map of the behavior variance regarding the EC of all recording vehicles. This energetic map includes the driving profile's influence on the EC regarding realized velocities and dynamics. This influence includes local factors like junctions and the visibility of curves as well as traffic, which cannot be further distinguished. The traffic information includes daytime and weekday dependent changes. Prospectively, a further adaption based on real time traffic information can be considered. This would enable the incorporation of short-term and unforeseeable events. Still, there are regular patterns in traffic flow and achievable speeds that reoccur. They can be seen in the data that is provided by the EPF. In this article, we aim to focus on the modeling of these effects during a long distance trip the traffic can significantly change along the route. Consequently, historical traffic information can be more reliable for initial planning of route sections passed several hours later.

For a given and segmented route H), the time- and segment-specific DPMADs I) are sent G) to the vehicle. However, some DPMADs might not be available for the required time or segment or both due to missing suitable fleet data recordings. In these cases, a multilevel backup applies. The levels are suitable sublink and time (no backup), suitable sublink, nearby sublink, and no data. In the suitable sublink case, there is just a lack of the needed time-specific recordings. Then the backup-DPMADs aggregate all recorded DPMAs at any time on the required segment. If there are furthermore no recordings on the required segment, the nearby sublink backup-DPMADs incorporate recordings of any time of 10 neighboring segments with the same speed limit and road type. In the rare event no data with no recordings found, the backup constructs DPMADs, which represent a constant driving at speed limit velocity. The models described in Section II-E and Section II-F select from the DPMADs the DPMAs for each segment of the route, to perform the EC prediction K), and provide it to the optimizer, as Fig. 1 depicts.

The prediction uses the DPMAs to predict the EC for defined boundary conditions. These conditions include besides vehicle properties also the road slope taken from digital maps and surrounding parameters like weather. The parameter vector $\vec{p}_{\mathrm{vec}}$ defines the vehicle's driving resistance parameters for the vehicle. Here, a prospective weather model can modify air density ρ and rolling resistance f_t. Additionally, such a weather model can incorporate the influence of wind in the route vector $\vec{r}_{\mathrm{vec}}$ by modifying the ISVP an ISVR for each segment according to wind speed and direction taken from weather forecast. Another influence of the weather on EC is a varying power consumed by auxiliary consumers $P_{Aux,i}$, namely the tempering of the vehicle. A segment specific $P_{Aux,i}$ adaption based on a tempering model including a weather forecast. The weather model will be part of future work, as this article focuses on the collaboration and interrelations of the optimizer and the EC prediction model.

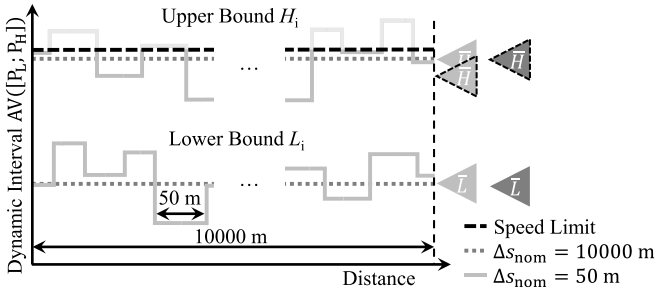

FIGURE 4. Principle of fleet-sourced velocity bounds and speed limit restriction.

E. VELOCITY BOUNDS BASED ON FLEET DATA

The optimization algorithm in Fig. 1 is fed with two different information by the EC. These are the velocity bounds L_i and H_i on one hand, and the corresponding energies for the given segment and velocity on the other hand. The energy consumption is provided by two different models: the ECM and the EPF. In turn, the velocity bounds itself are the basis for the EC calculation and only the EPF provides them.

Each segment's distribution of average velocity (DPMAD of AV) is the basis to select achievable speeds as optimization limits. Given that DPMADs are often non-Gaussian or bimodal, this selection utilizes percentile values and not statistical measures like standard deviation. For different scenarios, the selection uses a dynamic interval (DI) represented by the percentiles $P(H_i)$ and $P(L_i)$ to get the respective upper H_i and lower L_i velocity bounds.

As some drivers of the fleet might exceed the speed limit slightly, the EPF limits the upper bound by the segment-specific speed limit before providing it to the optimizer. This limitation prevents a suggestion non-legal speeds already on the level of strategy calculation.

Fig. 4 describes the resulting bounds for the EPF's Δs_{nom} of 50 m and a rougher value of 10 000 m. It depicts the typical effects on the derived bounds L_i and H_i and their distance-weighted mean values $\bar{L}$ and $\bar{H}$. For the lower bound, the EPF returns them with a finer spatial resolution, which gets averaged by the DPMAD's aggregation for the rougher Δs_{nom}. However, the mean $\bar{L}$ of all L_i stays approximately the same for both Δs_{nom}. For the upper bound, the speed limit affects $\bar{H}$. For the EPF's Δs_{nom}, the location-specific finer H_i exceeds the speed limit more often, which is then limited which the grayed out graph indicates. Still, it also shows a variation to lower speeds. Consequently, the speed limitation lowers $\bar{H}$, due to higher weighted lower speed variations, which the overlaying triangle indicates colored like the Δs_{nom} of 50 m line and framed like the speed limit line. In turn, the H_i with a rougher Δs_{nom} is already on the level of DPMADs averaged, which lowers $\bar{H}$ less due to speed limitation than for the finer EPF Δs_{nom}. In summary,

the incorporation of speed limits leads to lower $\bar{H}$ values for finer Δs_{nom}.

Moreover, this one-sided effect on the mean velocity bounds $\bar{L}$ and $\bar{H}$ limits the decision space to set wider bounds by $P(H_i)$ and $P(L_i)$. Accordingly, if the same amount increases the $P(H_i)$ as it lowers the $P(L_i)$, the value of $\bar{L}$ drops more than the value of $\bar{H}$ increases.

The second input of the EPF for the optimizer is the EC prediction itself. The EPF is designed to incorporate a percentile-based driver-classification for each DPMAD, which enables a customized EC prediction by using characteristics from a driver behavior as model input. However, this article aims to show a general idea of an optimal charging and driving strategy based on fleet data. Therefore, the driver-classification for the EC prediction uses the estimate for the most common driver, which relates to the median. The medians of each DPMA out of the DPMAPs are the basis for the EC prediction based on (12) and (13). This prediction of the most likely EC is the basis for the input to the optimizer. The next section details this collaboration.

F. MERGING VELOCITY AND FLEET-BASED CONSUMPTION PREDICTION

The information in Section II-D and Section II-E on consumption prediction and velocity bounds is now merged in segment-specific and speed-dependent ECs. Within segment-specific velocity bounds, the optimizer needs the EC for discrete points of possible mean velocities. For the EC, more than just the average segment speed (i.e., AV) derived as a median value from the fleet data has to be considered. ISVP (integral squared velocity while propulsion) and ISVR (integral squared velocity during recuperation) as well as IAP (integral acceleration while propulsion), and IAR (integral acceleration while recuperation) are the other DPMAs (energetic driving profile map attributes) for the calculation of an EC or energy demand with the EPF. For the most probable EC calculation, the EPF derives these DPMAs as the median out of the fleets' distribution. This is just valid together with a median fleet sourced speed AV. To resolve this, the DPMAs need to be modified for given AVs within the velocity bounds on a segment. This section investigates to what extent these DPMAs are a function of AV.

The acceleration-dependent IAP and IAR represent the dynamics' impact on EC on a specific segment. The speed-adaption of IAP and IAR is disregarded, as no speed-dependency of dynamics is noticeable. An analysis of the fleet-sourced IAP and IAR over AV showed a negligible dependency with a smaller than $2.5 \cdot 10^{-3}$ R-squared coefficient of determination. Thus, the fleet-derived median value for IAP and IAR is assumed for all AVs on a segment. This assumption is supported by the fact that velocity suggestions only should be made within velocity bounds higher than 70 km/h. For these higher velocities, the aerodynamic influence dominates the EC, which the quadratic velocity parameters ISVP and ISVR represent. As a consequence, only ISVP and ISVR need adaptions for given AVs.

The ISVP and ISVR are according to their definition in Tab. 1 speed dependent. These two DPMAs represent the velocity's influence on EC due to aerodynamic resistance. Therefore, the adaption of ISVP and ISVR to a given velocity needs to consider the quadratic behavior of the aerodynamic resistance regarding speed changes.

The following derivation and notation in (14) until (19) depicts only the ISVP modification for a given AV in the propulsion case. These equations equivalently apply in the recuperation case for ISVR speed-modification. The subscript "O" refers to the original fleet-distribution-based median ISVP referring to the fleet-median velocity, which step I) of the EPF provides. In turn, the subscript "M" refers to the ISVP values modified for a given velocity. If an equation is applicable for both the original and modified, there is no subscript as in (15) and (17).

For the modification of the velocity related DPMAs to a given AV, some assumptions are necessary and explained in the following. For the velocity-modification the assumption is that the same proportions of these phases apply for a modestly modified velocity. Subsequently, (14) describes this assumption for the original and modified values.

$$\frac{\text{ISVP}_\text{O}}{\text{ISV}_\text{O}} \approx : \frac{\text{ISVP}_\text{M}}{\text{ISV}_\text{M}} \tag{14}$$

Here, (14) defines the ratios as the proportion of ISVP to the overall integral squared velocity ISV. This is approximately the sum of both, as (15) depicts.

$$\text{ISV} \approx : \text{ISVP} + \text{ISVR} \tag{15}$$

When (14) and (15) are transposed to ISVP_M, this results in (16) for the desired estimates $\widehat{\text{ISVP}}_\text{M}$ of ISVP_M.

$$\widehat{\text{ISVP}}_\text{M} = \text{ISVP}_\text{O} \cdot \frac{\text{ISVP}_\text{M} + \text{ISVR}_\text{M}}{\text{ISVP}_\text{O} + \text{ISVR}_\text{O}} \tag{16}$$

As the ISV_M as defined by (15) is not available, the velocity-modification needs an estimated $\widehat{\text{ISV}}_\text{M}$. Since the velocity-modification suggests an AV, according to (17) AV can help to get this estimate $\widehat{\text{ISV}}_\text{M}$.

$$\widehat{\text{ISV}} = \int \text{AV}^2 ds = \text{AV}^2 \cdot \Delta s \tag{17}$$

For the verification of this assumption, the original data can serve as a test of (17) using (15). However, (15) is not entirely valid. This is due to the required interpolation while extracting the median DPMA and the quadratic nature of the variables. Nevertheless, it can be assumed that the ratio of this estimate $\widehat{\text{ISV}}_\text{M}$ to the real sum of ISVP_M and ISVR_M is not varying substantially for a modest velocity adaption, as (18) depicts.

$$\frac{\widehat{\text{ISV}}_\text{O}}{\text{ISVP}_\text{O} + \text{ISVR}_\text{O}} \approx : \frac{\widehat{\text{ISV}}_\text{M}}{\text{ISVP}_\text{M} + \text{ISVR}_\text{M}} \tag{18}$$

$$\widehat{\text{ISVP}}_\text{M} = \text{ISVP}_\text{O} \cdot \frac{\text{AV}_\text{M}^2 \cdot \Delta s}{\text{AV}_\text{O}^2 \cdot \Delta s} \tag{19}$$

Eq. (18) is rearranged for ISV_M and inserted into (16). Then, (18) simplifies the estimate calculation of $\widehat{\text{ISVP}}_\text{M}$

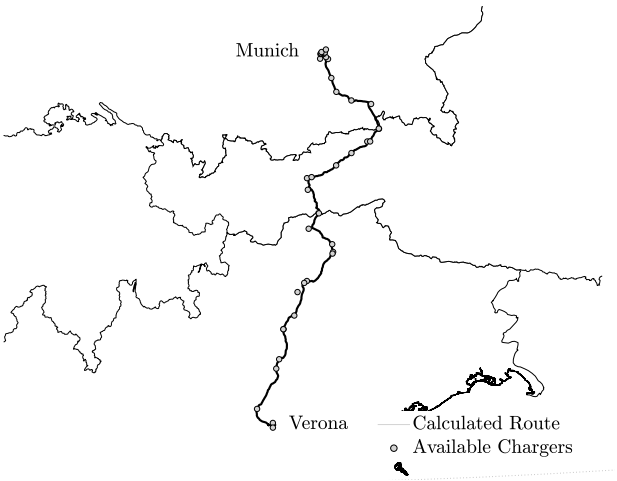

FIGURE 5. Provider-based Route from Munich to Verona incl. 39 chargers.

to (19). Overall, the DPMA modifications from an initial median estimate to a different given velocity described in this section, allow the EPF to provide a fleet-based and route-specific EC lookup-table over a velocity band. This table enables the optimizer to incorporate the speed-consumption trade-off for strategy planning.

G. ROUTE SCENARIO

As pointed out in Fig. 1, the underlying driving task is a fastest route provided by [22] from Munich in Germany to Verona in Italy. It is assumed that the charging infrastructure is sufficient so that the route choice still is time-optimal for fully electric vehicles. During this crossing of the European Alps, higher slopes and an alternation of national speed limits makes the task more versatile. It is 425 km long and provides a total of 39 charging stations along the way. These charging stations have nominal powers ranging from 50 to 120 kW. The latter is a hard-set limit, since it is the maximum charging power of the used charging model. The properties of the chargers originate to [28]. Possible detours from the given route are calculated through [22] and added to the cost function in (1) if a charging event is planned at a set charger. The charging time as well as the energy consumption of the vehicle, i.e., energy for driving and auxiliaries, depend on the ambient temperature. For the entire route task, environmental conditions are set to 20°C and applied to all models. The route consists of 1937 individual IDs and is then structured into sublinks, i.e., segments, with a maximal length of 50 m. However, there can be shorter segments, if there are changes in map data such as the speed limit, or the end of an ID. This results in a total number of 8992 segments, according to the finest discretization available from the EPF. For these segments, the EPF uses 601 639 km of driving data recorded from April and May 2018 to provide their information to the optimizer. Depending on the optimization scenario, they can be aggregated to longer segments. In the present case, this happens for a maximum nominal length of 10 000 m. The optimizer then uses this segment specific data and discretely controls speed and charging decisions (if possible) at the beginning of every new segment. Here, it is ensured that a set lower energy threshold $E_{\min}$ for the energy E_i in (7) is never undercut. It is set to 20 % SOC of the HVB. The optimization problem in (1) defines for every vertex i a possible charging event by defining the interval for r_i in (9). In the given route problem, for the majority of vertices i there is no charger. This has no impact on the optimization algorithm except that $\underline{r}_i$ is automatically set to zero if no charger is present.

III. SIMULATION & RESULTS

The previous chapter outlined the approach to derive a time-optimal strategy for a BEV on a given route. Firstly, the following sections illustrate the effects of a fine and a rough nominal route segmentation Δs_{nom} and of different velocity bounds based on a set moderate and very wide DI. Then, a comparison depicts the differences in these effects for the two described energy prediction inputs ECM and EPF. Only the latter incorporates fleet-based and segment-specific dynamics. Finally, the impact of different departure times on optimizer inputs and resulting strategies concludes the evaluations.

A. CONSUMPTION AND VELOCITY INPUT FOR OPTIMIZATION

For the driving task in Section II-G, the fleet-sourced velocity data and energy consumption data are generated for 08.30 a.m. on a weekday. They are then given to the optimizer, as shown in Fig. 1. For the analysis, two energetic scenarios are optimized, basing on ECM and the fleet-sourced EPF. However, both approaches use the same velocity data with a lower L_i, upper H_i and median value per segment that are derived by the EPF. The corresponding input data for a $\Delta s_{\text{nom}} = 50$ m can be seen in Fig. 6. Fig. 6(a) shows the distribution of the specific energy consumption per segment over the corresponding median velocity per segment as a boxplot for both energetic models. The median consumption values for ECM scatter less than the EPF data. Generally, the EPF based energy consumption is slightly higher in its median value than the ECM median for a given velocity. This is due to the additional segment-specific dynamics imposed in the EPF. Fig. 6(b) shows the occurrences as relative frequencies of median velocities in all segments. It can be seen that the higher the relative frequency for a given speed, the less the corresponding consumption data scatter.

The most frequent median velocities that are realized are 100, 110 and 130 km/h. This is because of speed limits in Germany, Austria and Italy. Also, the upper limit of speeds for the optimization of strategy is 130 km/h which refers to the speed German legislation recommends for sections with no speed limit. The velocities different from the ones named above are transition phases featuring more dynamics. Also, effects due to traffic are possible but cannot be quantified, as pointed out in Section II-D. In contrast, the more frequent

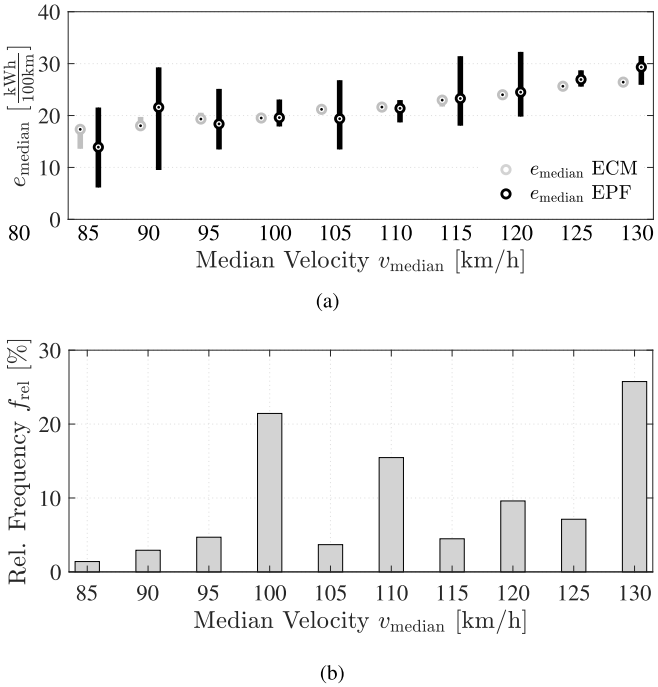

FIGURE 6. (a) Boxplot for the energy demand for fleet-based median velocities (only inter-quartile range and median depicted) and (b) its frequency.

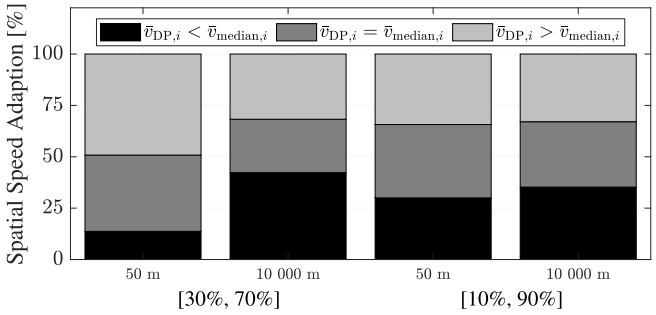

FIGURE 7. Way-based ratios of speed adaption in segmentation scenarios of 50 m and 10 000 m and two DIs of [10%, 90%] and [30%, 70%].

velocities refer to almost constant driving. This results in lower dynamics and thus less scatter in energy consumption. The next section investigates how the speed choice of the strategy calculation compares to the median speed values of the input data set.

B. STRATEGY OPTIMIZATION WITH THE CONSUMPTION MAP MODEL

The effect of fleet-based VWs around median speeds on the optimization is investigated. For energy consumption prediction, the ECM from Section II-D is used. The ECM provides energy consumption based on slope and velocity. For the distribution of vehicle speeds, the data from Section II-E is assumed as input.

The optimization is applied to the route scenario from Section II-G. To assess the effect of fleet-based VWs, two different segmentations (50 m and 10 000 m) as well as two DI scenarios ([10%, 90%] and [30%, 70%]) are optimized. The segmentation levels correspond to the highest resolution the EPF can provide, namely 50 m segments, and a comparably rough 10 000 m segmentation. In turn, the DI scenarios include a smaller, thus, conservative and wider characteristic. The latter provides more decision flexibility for the sake of less probability to be realizable while driving the route.

Fig. 7 shows the way-based speed adaption shares of the optimizer's velocity for the route task. The speed choice $v_{\text{DP},i}$ is compared to the median velocity $v_{\text{median},i}$ on every vertex i. The shares of covered distance where the optimizer's decision $v_{\text{DP},i}$ is greater, equal or less than the median $v_{\text{median},i}$ are shown in light gray, gray and black. By that, the effects of segmentation and DI on strategy calculation can be shown. The mean optimizer speeds $\bar{v}_{\text{DP},i}$ higher than the mean median $\bar{v}_{\text{median},i}$ are colored in light gray. They remain roughly constant, apart from the case for a distance segmentation of $\Delta s_{\text{nom}} = 50\,\text{m}$ and a dynamic interval of $[30\%, 70\%]$. Here, slightly less than 50 % of the entire driving task cover a higher mean speed than the median value. Consequently, the share of $\bar{v}_{\text{DP},i} < \bar{v}_{\text{median},i}$ in black decreases significantly to slightly more than 10 % in comparison to the other scenarios. The share of identical speeds in mid-gray also differs case-sensitively. The share is slightly higher when the discrete segmentation is finer. This is due to rounding effects discussed in Section II-E.

However, the higher ratio of speeds bigger than the median for the aforementioned left case makes sense when considering Tab. 2. For the results in this Section III-B that base on ECM, consider only the non-bold results. Here, only for the $\Delta s_{\text{nom}} = 50\,\text{m}$ and $[30\%, 70\%]$ case, two charging stops I and II are planned. Also, the mean optimizer velocity $\bar{v}_{\text{DP}}$ is comparably higher than for the other cases. Two factors cause the occurrence of two charging events. The discrete segmentation level of 50 m offers a detailed strategy optimization. Eq. (1) minimizes overall traveling time by continuously lowering the speed. However, the fine resolution for $\Delta s_{\text{nom}} = 50\,\text{m}$ and the resulting lower speed border of the 30 % percentile is not sufficient enough, to lower the speed that much, that the energy consumption does not demand the second charging stop II.

For the broader DI $[10\%, 90\%]$, and a lower $\bar{L}$ of 89.1 km/h rather than 101.7 km/h, the second charging stop can be prevented. For a rougher segmentation of 10 000 m, the effect described in Fig. 4 steps in: especially the slightly lower $\bar{L}$ prevents a second charging stop II. Due to aggregation, the upper and lower mean limits $\bar{H}$ and $\bar{L}$ differ. Apart from the $\Delta s_{\text{nom}} = 50\,\text{m}$ and $[30\%, 70\%]$, the charging strategies with a single stop in the other driving scenarios remain identical. The fewer segments, the broader the mean speed window, and consequently, the higher the mean optimizer speed $\bar{v}$ and the lower the overall traveling time $\sum \tau_i$.

The dynamic intervals also affect strategy optimization. A wider DI of $[10\%, 90\%]$ leads to an increased $\bar{v}$ and a lower overall traveling time, whereby the $\bar{L}$ mainly causes this dependency. However, from a probabilistic view, strategy

TABLE 2. Optimization results for consumption map based EPM input and differences for EPF based (bold).

DI	Dynamic Interval		$[30\%, 70\%]$				$[10\%, 90\%]$			
Δs_{nom}	Distance Segmentation		50 m		10 000 m		50 m		10 000 m	
$\Delta \underline{E}_i$	Discretization State Variable SOC		0.5%		0.5%		0.5%	0.01%	0.5%	
m	Number of Segments		8992		106		8992		106	
t_{calc}	Calculation time		2.8 h		122.4 s		3.06 h	3 d	134.8 s	
$\bar{H}$	Mean Upper Speed Bound [km/h]		112.8		114.4		114.5		115.5	
$\bar{L}$	Mean Lower Speed Bound [km/h]		101.7		101.4		89.1		87.2	
$\bar{v}_{\text{DP}}$	Mean Optimized Speed [km/h]		111.0	**-1.5**	108.8	**-2.9**	107.9	**-1.8**	**-1.3**	109.6	**-2.6**
$n_{\tilde{i}}$	Charging Event		I + II	≡	I	≡	I	**+II**	≡	I	≡
$r_{\tilde{i}}$	Final Charging SOC [%]	I	98.5	**+1.0**	100	**±0.0**	99.0	**+1.0**	**+1.0**	100.0	**±0.0**
		II	28.0	**±0.0**	-	-	-	**+27**	-	-	-
$\Delta r_{\tilde{i}}$	Charged SOC per Event [%]	I	50.0	**+3.0**	51.0	**+3.0**	51.0	**+1.5**	**+2.4**	52.0	**+2.5**
		II	5.0	**+0.0**	-	-	-	**+0.5**	-	-	-
$\sum \tau_i$	Overall Traveling Time [min]		319.7	**+5.4**	298.4	**+9.2**	301.7	**+27.7**	**+5.2**	297.4	**+6.9**

planning gets more and more insecure due to the wider VWs and a less precise prediction for the most probable fleet behavior. The given results illustrate the importance of the lower velocity bound for a time-minimal solution, especially for wider intervals. It is yet to analyze, to which extent additional fleet-sourced ECs due to the application of the EPF's energetic part enforce this effect.

Lastly, the fine spatial discretization in $m = 8992$ segments for $\Delta s_{\text{nom}} = 50\,\text{m}$ leads to what is commonly known as the *Curse of Dimensionality* for DPs [25]. Due to the highly detailed model and the matrix-based evaluation of DP, calculation times t_{calc} for these use cases are comparably high with a total of 2.8 h for $[30\%, 70\%]$ and 3.06 h for the broader dynamic interval $[10\%, 90\%]$. A wider DI results in higher calculation times, as the optimizer evaluates a broader velocity window and thus a higher number of discrete decisions. Due to comparisons in terms of EC model, the authors also had to re-calculate a fine spatial discretization use-case of $\Delta s_{\text{nom}} = 50\,\text{m}$ and a DI of $[10\%, 90\%]$ with a finer state resolution. This resulted in an even higher computation time of 3 days. However, for a spatial segmentation of $\Delta s_{\text{nom}} = 10\,000\,\text{m}$, and thus $m = 106$ segments, the computation times become significantly smaller. This means 122.4 s and 134.8 s for $[30\%, 70\%]$ and $[10\%, 90\%]$, respectively. All optimizations have been executed on conventional hardware with an Intel i7 with 1.9 GHz and a RAM of 16 GB. To reduce that number even more, backend-based optimization for the rougher segmentation of $m = 106$ can be a solution for real-time applications.

C. DIFFERENCES IN APPLICATION OF FLEET CONSUMPTION MODEL

For illustrating the difference in both the ECM and EPF approach, the optimization algorithm uses the fleet-based energy consumption values that base on the EPF. In addition to a dependency of energy consumption on segment length, slope, and speed in the ECM, segment specific dynamics from the fleet are added to the energy consumption in the EPF case. This includes breaking, i.e., recuperating, as well as accelerating locally.

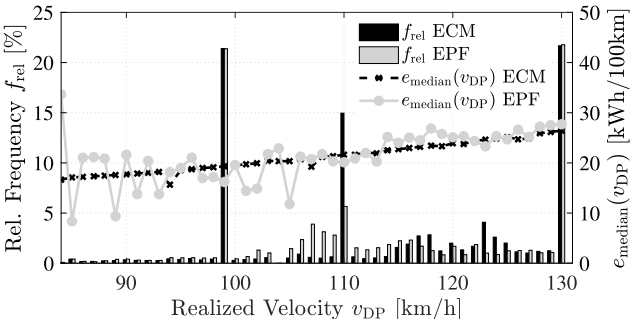

FIGURE 8. Bar graph of share of realized vehicle speeds for the ECM (black) and EPF (white) case for $\Delta s_{\text{nom}} = 50$ m and [30%, 70%] and $\Delta e_{\text{median}}\,(v_{\text{DP}})$ for the speed-dependent ECM and EPF consumption medians.

The optimization scenario is identical to the ECM case. Again, two distance segmentation levels $\Delta s_{\text{nom}} = 50\,\text{m}$ and 10 000 m and two DIs ($[10\%, 90\%]$ and $[30\%, 70\%]$) are applied. The numeric results are found in bold in Tab. 2. Generally, an identical charging strategy setting is optimized, excluding the strategy for the $\Delta s_{\text{nom}} = 50\,\text{m}$ and $[10\%, 90\%]$ case. Linearization errors in the calculation of control variables for the state space grid lead to a strategy deviation. These effects have already been described in [12]. Thus, for a better comparison of both ECM and EPF, a finer state space grid discretization of $\Delta \underline{E}_i = 0.01\,\%$ is chosen for more comparable results. Generally, the additional energy in the prediction model through dynamics provokes more conservative planning. This leads to lower mean optimized speeds $\bar{v}$ and consequently to higher overall travel time. Also, a higher charged SOC leads to pro-longed charging processes in comparison to the ECM case. Additionally, both ECM and EPF provoke different effects on strategy optimization. For that, the realized speeds in the driving task and corresponding energies are analyzed in detail. Fig. 8 shows the distribution of planned velocities with a black and gray histogram for ECM and EPF, respectively.

This is done for a discrete segmentation of $\Delta s_{\text{nom}} = 50\,\text{m}$ and a DI of $[30\%, 70\%]$. Correspondingly, the ECs are given as medians relating to the realized speeds over the entire driving task. For velocities with fewer occurrences, i.e., lower

relative frequencies, the median energy values vary more. This behavior can also be seen in Fig. 4 for low ratio speeds. Three local maxima of realized speeds can be identified for both prediction models: 99 km/h, 110 km/h and 130 km/h. These velocities represent the optimizer's handling of speed limits along the given route task. The medians for the EPF cases for these speeds are either slightly smaller (99 km/h, 110 km/h) or higher (130 km/h) than the equivalent ECM value. Normally, when adding dynamics to a non-dynamic energy value, the behavior of the latter is expected: an EPF-median higher than the ECM value. The fact that the energy medians for the EPF approach are smaller than the ECM data for 99 km/h and 110 km/h originates to breaking or additional recuperation due to slope. They are not taken into account for the ECM case.

In total, the EPF is more precise, as it incorporates vehicle dynamics. These lead to an additional consumed energy of 1.8 - 2.3 % compared to the ECM for the different optimization settings. Therefore, the mean velocities are lowered for the EPF case. Consequently, this results in an elongation of 5.2 min - 9.2 min. Due to the more precise EPF, the optimization result are more robust in real driving use cases. The derived charging strategies are the same for EPF and ECM input, as the optimizer can reduce EC enough to compensate the additionally modeled dynamics by lowering the mean velocity to reach the same chargers.

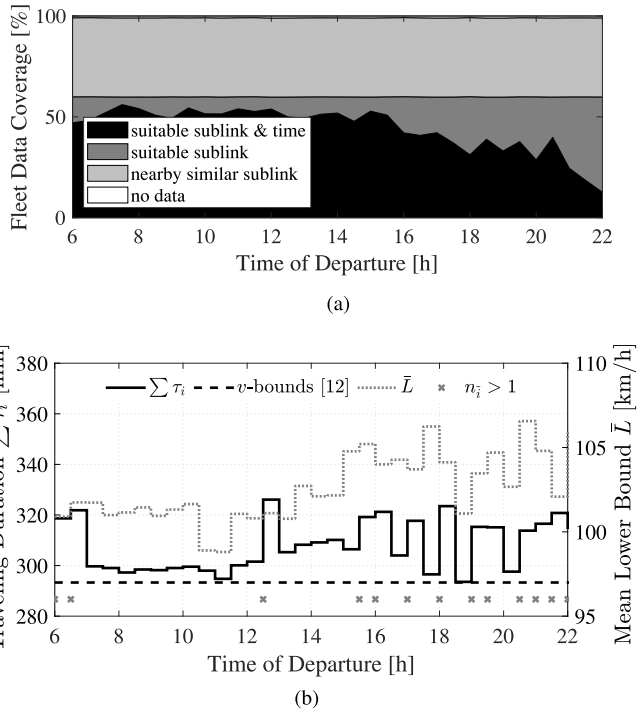

FIGURE 9. **(a) Fleet data coverage, (b) mean lower velocity bound from fleet data, total travel duration, and number of charging events greater one subject to the time of departure from Munich to Verona.**

D. DEPENDENCY OF STRATEGY OPTIMIZATION ON DEPARTURE TIME

The final evaluations vary the departure time of the driving task from Munich to Verona in increments of half an hour from 06.00 a.m. to 10.00 p.m. This evaluation displays time-dependent changes in the velocity bounds and its effect on strategy calculation. Therefore, the respective fleet-sourced velocity bounds are derived using the moderate DI of $[30\%, 70\%]$ for each segment at the corresponding time on it. Based on these bounds, an optimization following (1) calculates optimal velocities, charging stops and charging energies. This is done for every departure time. Here, the optimization with a nominal distance discretization $\Delta s_{\text{nom}} = 10\,000\,\text{m}$ utilizes the ECM. Fig. 9(a) depicts the ratios of applied backup levels due to fleet data coverage for each departure time, as described in Section II-D.

It shows that only seldom fleet data are unavailable. The highest quality of fleet data is available for departures until 05.00 p.m. Due to four to five hours of traveling time, later departures lead to arrivals in Verona at night-times. Less traffic in the night leads to a relatively lower degree of available fleet data. Consequently, a larger ratio of the derived velocity bounds for these times gets replaced by neighboring data, as depicted in Section II-D. More than the used fleet data of two months, as Section II-G depicts, would be necessary for a better resolution. Consequently, the interpretation of the optimizer's results needs to consider this averaging in the night-time.

Subsequently, Fig. 9(b) shows the relevant fleet-sourced velocity information and the optimizer results over departure time. It displays only the lower velocity bound $\bar{L}$, as the previous evaluations showed that it has the biggest influence on the driving strategy. This is due to the fact that the upper bound is varying less due to speed limitation (see Fig. 4). The departure until midday from Munich tends to be more influenced by rush hour traffic resulting in lower velocities. In turn, the velocities of the arrival in Verona, which rush hour traffic also could affect, are less lowered. This is potentially due to the anti-cyclic arrival. As previously discussed, late departures are neglected due to limited data quality. For earlier departures, the differences in the lower velocity bound force the optimizer to increase the number of charging stops $n_{\bar{i}}$ to two, as the previous evaluations showed. Thus, for departures with higher accessible $\bar{L}$ for the driver, the optimizer needs to incorporate an additional charging stop, which results in a longer overall duration of travel $\sum \tau_i$ if the driver cannot drive a lot faster. Due to off-peak traffic, local minima in total travel time are reached for departures at 11.30 a.m. and 06.30 p.m., whereas the latter might suffer from insufficient data coverage. This effect has already been mentioned above.

Lastly, the dashed-line of a constant total travel time of 295 min represents a benchmark based on the scenario that has been described in [12]. There, instead of time-and location specific velocity bounds from the fleet fixed speed bounds were assumed. The upper limit H_i was modeled as the

tempo limit on road segments. The lower limit L_i was an offset of 50 km/h to the upper bound. In the present paper, this way of defining velocity bounds is transferred to the given driving use case and compared to fleet-based velocity bounds throughout an entire day. This time-dependent comparison of total driving times can be seen in Fig. 9(b). Obviously, the adapted speed bounds from [12] stay identical. Since fleet-based velocity bounds reflect time-dependent variation, the derived strategies are less optimistic than the fixed one from [12]. Additionally, they vary in total driving time and necessity of charging stops, which cannot be reflected by the less realistic tempo-limit-based bounds. The consequence in real driving applications combined with tempo-limit bounds would be an underestimation of constraints and deviations of up to 11 % in total driving time at 12.30 a.m.

IV. CONCLUSION

The goal of this article was to combine the optimization of long distance trips for BEVs with a fleet-based energy consumption model to derive realistic strategies minimizing overall traveling time. The focus was to compute a strategy that is as realistic as possible. To guarantee that, planning of charging stops and energies as well as vehicle speed was enabled. Accordingly, a non-linear charging model calculated charging time as a function of charged energy. For viable speed suggestions by the optimizer, the fleet data provided realistic location- and time-specific velocity bounds. In order to evaluate these speed adaptions energetically, two energy consumption models were used. A conventional consumption map model and a fleet-sourced energy consumption prediction. For the latter, the velocities and dynamics from the fleet were used. This included 601 639 km of recorded and processed vehicle data on the given 425 km route scenario from Munich to Verona.

The present evaluations depicted the impact of different algorithm settings and departure times for the driving task. This included both a detailed and rougher spatial segmentation of the route, its corresponding calculation times as well as different widths for the fleet-sourced velocity windows. Due to legal speed limits, a broader velocity window mostly leads to a decreased lower accessible velocity bound, while the upper bound stays similar. As a result, the lower velocity limit mainly influences the optimizer's decision space and the amount of charging stops. Ultimately, it strongly reduces the overall driving time by up to 18 min. Still, the broader the velocity windows from the fleet, the less it tended to represent the most probable fleet behavior. The fleet-sourced approach including dynamics is more precise in comparison to the consumption map-based one. This led to higher energy consumption in most of the cases and thus a more robust prediction. Although the optimizer reacted to this additional energy consumption by reducing the velocity on average, the energy consumption increased by 1.8 - 2.3 % . However, the optimizer could keep the charger selection for both energy consumption models and thus compensated additional consumption by reducing speed resulting in a prolongation of 5.2 min - 9.2 min in total travel time. Finally, the effect of the departure time on strategy optimization was evaluated using time-dependent velocity windows. Here, the optimizer tended to vary the number of charging stops. This was caused by a limited decision space, mainly due to the lower velocity bound. A local minimum in terms of time-optimal departure time are at 11.30 a.m., resulting in about 297 min overall traveling time. A benchmark with a previous publication showed the importance of more realistic time-dependent speed bounds in strategy calculation with deviations of up to 11 %.

Future work will include a driver-specific adaption for more reliable velocity bounds including a real-time traffic adaption. More specific bounds can reflect the individual velocity selection habits of the driver within the overall fleet-behavior. Moreover, prospective work on the energy demand prediction will address the influences of weather (e.g., vehicle tempering, wind) and usage (e.g., trailer, mass) factors by incorporation of a weather forecast and driving resistance estimation. Furthermore, an application of the optimizer's selected speeds for autonomous driving will be evaluated. A suggestion of the appropriate speed will be crucial for ego-vehicles. In terms of route choice, an alternative framework that incorporates routing strategy in the optimization process is currently being developed and assessed. In terms of the optimization model itself, a benchmark to other algorithmic approaches will be evaluated in order to assess the performance and solution quality of the chosen DP approach.

Finally, the derived strategies based on the presented model framework lead to one-sided usage of the charger network and, consequently, the electricity supply system. Apart from a model to predict the availability of and waiting time for chargers, the interaction of the vehicle system and the electricity supply will be part of prospective work on the optimization algorithm.

REFERENCES

[1] *Traffic in Kilometers—National Traffic Load*, Kraftfahrt-Bundesamt, Berlin, Germany, 2018. Accessed: Mar. 3, 2020. [Online]. Available: https://www.kba.de/DE/Statistik/Kraftverkehr/VerkehrKilometer/verkehr_in_kilometern_kurzbericht_pdf.pdf

[2] F. Duffner, M. Wentker, M. Greenwood, and J. Leker, "Battery cost modeling: A review and directions for future research," *Renew. Sustain. Energy Rev.*, vol. 217, Jul. 2020, Art. no. 109872.

[3] A. Artmeier, J. Haselmayr, M. Leucker, and M. Sachenbacher, "The shortest path problem revisited: Optimal routing for electric vehicles," in *Proc. Annu. Conf. Artif. Intell. (KI)*, vol. 6359. Karlsruhe, Germany, 2010, pp. 309–316.

[4] J. Eisner, S. Funke, and S. Storandt, "Optimal route planning for electric vehicles in large networks," in *Proc. 25th AAAI Conf. Artif. Intell.*, San Francisco, CA, USA, 2011, pp. 1108–1113.

[5] M. Baum, J. Sauer, D. Wagner, and T. Zündorf, "Consumption profiles in route planning for electric vehicles: Theory and applications," in *Proc. 16th Int. Symp. Exp. Algorithms*, vol. 75. London, U.K., 2017, pp. 1–18.

[6] F. Baouche, R. Billot, R. Trigui, and N.-E. El Faouzi, "Electric vehicle shortest path problem with replenishment constraint," in *Proc. Int. Conf. Connected Veh. Expo*, Vienna, Austria, 2014, pp. 2787–2792.

[7] G. Huber and K. Bogenberger, "Optimal charging strategies for electric cars on long trips," in *Proc. 3rd Conf. Future Autom. Technol. (COFAT)*, Munich, Germany, 2014.

[8] S. Storandt, "Quick and energy-efficient routes: computing constrained shortest paths for electric vehicles," in *Proc. 25th AAAI Conf. Artif. Intell.*, Redondo Beach, CA, USA, 2012, pp. 20–25.

[9] T. Wang, C. Cassandras, and S. Pourazarm, "Energy-aware vehicle routing in networks with charging nodes," *IFAC Proc. Vol.*, vol. 47, no. 3, pp. 9611–9616, 2014.

[10] S. Pourazarm and C. G. Cassandras, "Optimal routing of energy-aware vehicles in transportation networks with inhomogeneous charging nodes," *IEEE Trans. Intell. Transp. Syst.*, vol. 19, no. 8, pp. 2515–2527, Aug. 2018.

[11] M. Baum, J. Dibbelt, L. Hübschle-Schneider, T. Pajor, and D. Wagner, "Speed-consumption tradeoff for electric vehicle route planning," in *Proc. 14th Workshop Algorithmic Approaches Transp. Model. Optim. Syst.*, vol. 42, 2014, pp. 138–151.

[12] M. Cussigh and T. Hamacher, "Optimal charging and driving strategies for battery electric vehicles on long distance trips: A dynamic programming approach," in *Proc. IEEE Intell. Veh. Symp. (IV)*, Paris, France, 2019, pp. 2093–2098.

[13] S. Sellschopp, "Predicting an energy consumption of a vehicle," Patent EP2 948 357 (A1), Dec. 2015.

[14] A. Lamprecht, "Energieprädiktion und reichweitenanzeige durch navigationsdaten," Ph.D. dissertation, Dept. Doktor-Ingenieur, Technische Universität Chemnitz, Chemnitz, Germany, 2015.

[15] S. Grubwinkler, T. Brunner, and M. Lienkamp, "Range prediction for EVs via crowd-sourcing," in *Proc. IEEE Veh. Power Propulsion Conf. (VPPC)*, Coimbra, Portugal, 2014, pp. 1–6.

[16] X. Qi, G. Wu, K. Boriboonsomsin, and M. J. Barth, "Data-driven decomposition analysis and estimation of link-level electric vehicle energy consumption under real-world traffic conditions," *Transp. Res. D, Transp. Environ.*, vol. 64, pp. 36–52, Oct. 2018.

[17] C. de Cauwer, W. Verbeke, J. van Mierlo, and T. Coosemans, "A model for range estimation and energy-efficient routing of electric vehicles in real-world conditions," *IEEE Trans. Intell. Transp. Syst.*, vol. 21, no. 7, pp. 2787–2800, Jul. 2020.

[18] J.-Y. Yang, L.-D. Chou, and Y.-J. Chang, "Electric-vehicle navigation system based on power consumption," *IEEE Trans. Veh. Technol.*, vol. 65, no. 8, pp. 5930–5943, Aug. 2016.

[19] J. Wang, I. Besselink, and H. Nijmeijer, "Battery electric vehicle energy consumption prediction for a trip based on route information," *Proc. Inst. Mech. Eng. D, J. Automobile Eng.*, vol. 232, no. 11, pp. 1528–1542, 2018.

[20] T. Straub, M. Nagy, M. Sidorov, L. Tonetto, M. Frey, and F. Gauterin, "Energetic map data imputation: A machine learning approach," *Energies*, vol. 13, no. 4, p. 982, 2020.

[21] M. Masikos, M. Theologou, K. Demestichas, and E. Adamopoulou, "Machine-learning methodology for energy efficient routing," *IET Intell. Transp. Syst.*, vol. 8, no. 3, pp. 255–265, May 2014.

[22] *Routing API V7*, HERE Global B.V., Amsterdam, The Netherlands, 2020. Accessed: Mar. 3, 2020. [Online]. Available: https://developer.here.com/documentation/routing/dev_guide/topics/request-constructing.html

[23] P. Newson and J. Krumm, "Hidden markov map matching through noise and sparseness," in *Proc. 17th ACM SIGSPATIAL Int. Conf. Adv. Geograph. Inf. Syst.*, Seattle, WA, USA, 2009, pp. 336–343.

[24] R. Bellman, "The theory of dynamic programming," *Bull. Amer. Math. Soc.*, vol. 60, pp. 503–515, Jul. 1954.

[25] D. Bertsekas, *Dynamic Programmig and Control: Volume 1*. Belmont, CA, USA: Athena Sci., 2005.

[26] O. Sundström and L. Guzzella, "A generic dynamic programming MATLAB function," in *Proc. IEEE Control Appl. CCA Intell. Control (ISIC)*, St. Petersburg, Russia, 2009, pp. 1625–1630.

[27] R. Korthauer, Ed., *Handbuch Lithium-Ionen-Batterien*. Berlin, Germany: Springer, 2013.

[28] *Open Charge Map: The Global Public Registry of Electric Vehicle Charging Locations*, Open Charge Map, 2020. Accessed: Mar. 3, 2020. [Online]. Available: https://openchargemap.org/

MAXIMILIAN CUSSIGH received the B.Sc. and M.Sc. degrees in mechanical and energy engineering from RWTH Aachen University in 2015 and 2017, respectively. He is currently pursuing the Ph.D. degree with BMW AG and Technical University Munich under the supervision of T. Hamacher. His research interests include electrified vehicle systems, operational strategies, navigation, and discrete optimization.

TOBIAS STRAUB received the B.Eng. degree in mechanical engineering from the Deggendorf Institute of Technology in 2015, and the M.Sc. degree in mechanical engineering from Ostbayerische Technische Hochschule Regensburg in 2017. He is currently pursuing the Ph.D. degree with BMW AG and KIT under the supervision of F. Gauterin. His research interests include electrified vehicle systems, vehicle energy demand, driver-assistance systems, and analysis of fleet-sourced big data.

MICHAEL FREY received the Diploma and Doctoral degrees in mechanical engineering from the University of Karlsruhe in 1993 and 2004, respectively. He is the Manager of the Research Group Automation and the Research Group Suspension and Propulsion Systems, Institute of Vehicle Systems Technology. His research interests are driver-assistance systems, operational strategies, suspension systems, vehicle dynamics, as well as vehicle modeling and optimization.

THOMAS HAMACHER is a Full Professor of renewable and sustainable energy systems with Technical University Munich, Germany. His research focuses on energy and systems analysis, focusing on urban energy systems, the integration of renewable energy into the power grid, and innovative nuclear systems (including fusion). Other focuses of his work are the methods and fundamentals of energy models.

FRANK GAUTERIN received the Diploma degree in physics from the University of Münster, Germany, in 1989, and the Dr. rer. nat. (Ph.D.) degree from the University of Oldenburg, Germany, in 1994. From 1989 to 2000, he worked as an Acoustics Engineer, and from 2000 to 2006, as the Director of the Noise Vibration and Harshness (NVH) Engineering Profit Centre, Continental AG, Hanover, Germany, with locations in Germany, USA, and Malaysia. Since 2006, he has been a Full Professor of vehicle technology with the Karlsruhe Institute of Technology (KIT), Germany, the Head of the Institute of Vehicle System Technology, and scientific spokesperson of the KIT Centre Mobility Systems. His research interests are vehicle conception, control, suspension and drive systems, tire road interaction, and NVH.